The conserved SNARE SEC-22 localizes to late endosomes and negatively regulates RNA interference in *Caenorhabditis elegans*

YANI ZHAO, BENJAMIN T. HOLMGREN, and ANDREA HINAS
Department of Cell and Molecular Biology, Uppsala University, 751 24 Uppsala, Sweden

ABSTRACT

Small RNA pathways, including RNA interference (RNAi), play crucial roles in regulation of gene expression. Initially considered to be cytoplasmic, these processes have later been demonstrated to associate with membranes. For example, maturation of late endosomes/multivesicular bodies (MVBs) is required for efficient RNAi, whereas fusion of MVBs to lysosomes appears to reduce silencing efficiency. SNAREs (soluble *N*-ethylmaleimide-sensitive factor attachment protein receptors) mediate membrane fusion and are thus at the core of membrane trafficking. In spite of this, no SNARE has previously been reported to affect RNAi. Here, we demonstrate that in *Caenorhabditis elegans*, loss of the conserved SNARE SEC-22 results in enhanced RNAi upon ingestion of double-stranded RNA. Furthermore, SEC-22 overexpression inhibits RNAi in wild-type animals. We find that overexpression of SEC-22 in the target tissue (body wall muscle) strongly suppresses the *sec-22(−)* enhanced RNAi phenotype, supporting a primary role for SEC-22 in import of RNAi silencing signals or cell autonomous RNAi. A functional mCherry::SEC-22 protein localizes primarily to late endosomes/MVBs and these compartments are enlarged in animals lacking *sec-22*. SEC-22 interacts with late endosome-associated RNA transport protein SID-5 in a yeast two-hybrid assay and functions in a *sid-5*-dependent manner. Taken together, our data indicate that SEC-22 reduces RNAi efficiency by affecting late endosome/MVB function, for example, by promoting fusion between late endosomes/MVBs and lysosomes. To our knowledge, this is the first report of a SNARE with a function in small RNA-mediated gene silencing.

Keywords: RNAi; late endosome; SNARE; *C. elegans*

INTRODUCTION

In RNA interference (RNAi), small RNAs are processed from longer double-stranded (ds) RNA by the endonuclease Dicer and subsequently incorporated into the RNA induced silencing complex (RISC). The small RNA guides RISC to complementary target mRNA, resulting in repression of gene expression (Ghildiyal and Zamore 2009). In the nematode *Caenorhabditis elegans*, RNAi can be induced by expressing transgenic dsRNA, injecting dsRNA, or by exposing the animals to environmental dsRNA by soaking them in dsRNA solution or feeding them bacteria that express dsRNA (Fire et al. 1998; Tabara et al. 1998; Timmons et al. 2001; Winston et al. 2002). Importantly, dsRNA-induced gene silencing spreads efficiently between cells and tissues in *C. elegans*, a phenomenon known as systemic RNAi (Fire et al. 1998; Winston et al. 2002). A forward genetic screen identified a number of proteins required for this process, termed SID (systemic RNAi defective) (Winston et al. 2002), all of which appear to be transmembrane or membrane-associated proteins (Winston et al. 2002, 2007; Hinas et al. 2012; Jose et al. 2012).

In addition to proteins required for RNA transport, core proteins of the RNAi machinery also appear linked to membranes, although the underlying details remain elusive. Dicer as well as the RISC component Argonaute were initially isolated biochemically as membrane-associated proteins (Cikaluk et al. 1999; Tahbaz et al. 2004), but it was not until a few years ago that this membrane association of Argonautes and other RISC proteins was further investigated (Gibbings et al. 2009; Lee et al. 2009; Stalder et al. 2013). RISC components have been reported to associate with the rough endoplasmic reticulum (ER) and with late endosomes/multivesicular bodies (MVBs) to facilitate RISC assembly and reassembly, respectively (Gibbings et al. 2009; Lee et al. 2009; Stalder et al. 2013). MVBs are formed during endosomal

Corresponding author: andrea.hinas@icm.uu.se
Article is online at http://www.rnajournal.org/cgi/doi/10.1261/rna.058438.116. Freely available online through the *RNA* Open Access option.

© 2017 Zhao et al. This article, published in RNA, is available under a Creative Commons License (Attribution-NonCommercial 4.0 International), as described at http://creativecommons.org/licenses/by-nc/4.0/.

maturation via inward membrane budding of intralumenal vesicles (ILVs) (Scott et al. 2014). In *Drosophila melanogaster* and mammalian cells, inhibition of MVB formation by knockdown of ESCRT (endosomal sorting complex required for transport) proteins was found to decrease RNAi as well as silencing by the related micro (mi)RNA pathway (Gibbings et al. 2009; Lee et al. 2009). Conversely, small RNA-mediated silencing was enhanced when fusion of MVBs to lysosomes was blocked (Lee et al. 2009; Harris et al. 2011). Later, autophagy of mammalian Dicer and Argonaute 2 and *C. elegans* AIN-1, a homolog of another core RISC protein, GW182, has been demonstrated to negatively regulate miRNA silencing (Gibbings et al. 2012; Zhang and Zhang 2013). The maturation pathways of late endosomes/MVBs and autophagosomes are closely intertwined, and at present, it is not clear to what extent the functions of these compartments in RNAi and miRNA silencing are connected, although they do not appear to be completely overlapping (Voinnet 2013).

With their crucial function in vesicle fusion, soluble *N*-ethylmaleimide-sensitive factor attachment protein receptors (SNAREs) are at the core of intracellular membrane trafficking. In the classic example, an R-SNARE (also referred to as vesicle [v-]SNARE) residing in one membrane forms a *trans*-SNARE complex with Q-SNAREs (or target [t-]SNAREs) from another membrane, thereby promoting membrane fusion (Ungar and Hughson 2003). Despite the central role of SNAREs in membrane fusion, no SNARE has previously been implicated in small RNA silencing. We previously showed that the putative transmembrane protein SID-5 localizes to late endosomes/MVBs and promotes transport of RNAi silencing signals between cells in *C. elegans* (Hinas et al. 2012). In the present study, we identify the conserved R-SNARE SEC-22 in a yeast two-hybrid (Y2H) screen using SID-5 as bait. We show that *sec-22* negatively regulates RNAi in a *sid-5*-dependent manner and that this inhibition primarily affects RNA import or cell autonomous RNAi. We find that SEC-22 colocalizes mainly with late endosomal/MVB proteins and that loss of SEC-22 results in enlarged late endosomes/MVBs. Taken together, this supports a model where SEC-22 acts at late endosomes/MVBs to reduce RNAi efficiency, for example, by promoting, directly or indirectly, fusion to lysosomes. To our knowledge, this is the first report of a bona fide SNARE with a function in RNAi.

RESULTS AND DISCUSSION

The *C. elegans* SNARE SEC-22 interacts with RNA transport protein SID-5 in a yeast two-hybrid screen

We identified the R-SNARE SEC-22 as a putative binding partner of the RNA transport protein SID-5 in a Y2H screen modified for membrane proteins (Stagljar et al. 1998). SEC-22 is one of two *C. elegans* longin SNAREs, proteins containing a regulatory so-called longin domain and a coiled-coil/synaptobrevin domain, and is conserved throughout eukaryotes (Fig. 1A,B, Supplemental Fig. S1; Filippini et al. 2001). While vertebrates have three SEC-22 paralogs (A–C), *Saccharomyces cerevisiae, C. elegans,* and *D. melanogaster* each possess a single SEC-22 ortholog (Fig. 1B; Supplemental Fig. S1). The canonical role of SEC-22 SNAREs is to promote trafficking between the ER and Golgi compartments (Barlowe and Miller 2013). However, the functional repertoire of SEC-22 homologs has more recently been expanded. Specifically, mouse Sec22b has been demonstrated to localize to the ER–Golgi intermediate compartment (ERGIC) to deliver ER proteins to phagosomes in dendritic cells (Cebrian et al. 2011). In addition, human Sec22b as well as *S. cerevisiae* Sec22 can mediate ER–plasma membrane contact in a nonfusogenic manner, facilitating membrane expansion during cell growth (Petkovic et al. 2014). In *C. elegans*, SEC-22 has not previously been investigated apart from the observation that SEC-22 depletion by RNAi results in increased accumulation of α-synuclein::GFP aggregates and neurodegeneration in a Parkinson model (Hamamichi et al. 2008).

C. elegans sec-22 mutants display enhanced RNAi

Confirmation of physical protein–protein interactions detected in Y2H assays is commonly achieved by coimmunoprecipitation. However, coimmunoprecipitation of transmembrane proteins can be challenging, and therefore the transmembrane domain(s) are often removed prior to analysis. Since SID-5 is a protein of only 67 amino acids with the transmembrane domain situated in the middle, this approach is not possible and we have thus not confirmed the possible physical interaction between SID-5 and SEC-22. Instead, we focused on the possible role of SEC-22 in RNAi. To this end, we assayed a *sec-22(ok3053)* deletion mutant, from here on referred to as *sec-22(−)*, for response to bacteria-mediated (feeding) RNAi. In contrast to *sid-5* mutants, which show reduced RNAi (Hinas et al. 2012), we found that the *sec-22 (−)* mutant displayed enhanced sensitivity to RNAi (Eri phenotype). The *sec-22(−)* mutant showed stronger RNAi responses compared to wild-type animals when fed bacteria expressing dsRNA targeting the epidermis-expressed *dpy-13* gene (Fig. 1, C and D), body wall muscle-expressed gene *unc-22* (Fig. 1E), as well as intestine-expressed gene *act-5* (Fig. 1F). The enhanced RNAi phenotype could be rescued by an extrachromosomal array carrying the *sec-22* gene and a few hundred base pairs of flanking sequence (*sec-22p::sec-22*, Fig. 1C,E). Enhanced RNAi was also observed in *sec-22 (−)* animals upon feeding RNAi against a body wall muscle-expressed GFP transgene (Fig. 1G,H). Importantly, we furthermore observed enhanced RNAi against *dpy-13* and *unc-22* in a strain carrying an independent mutant allele, *sec-22(gk887451)*, which substitutes glutamic acid 2 for lysine (E2K, Fig. 1I,J). It should be noted that although the

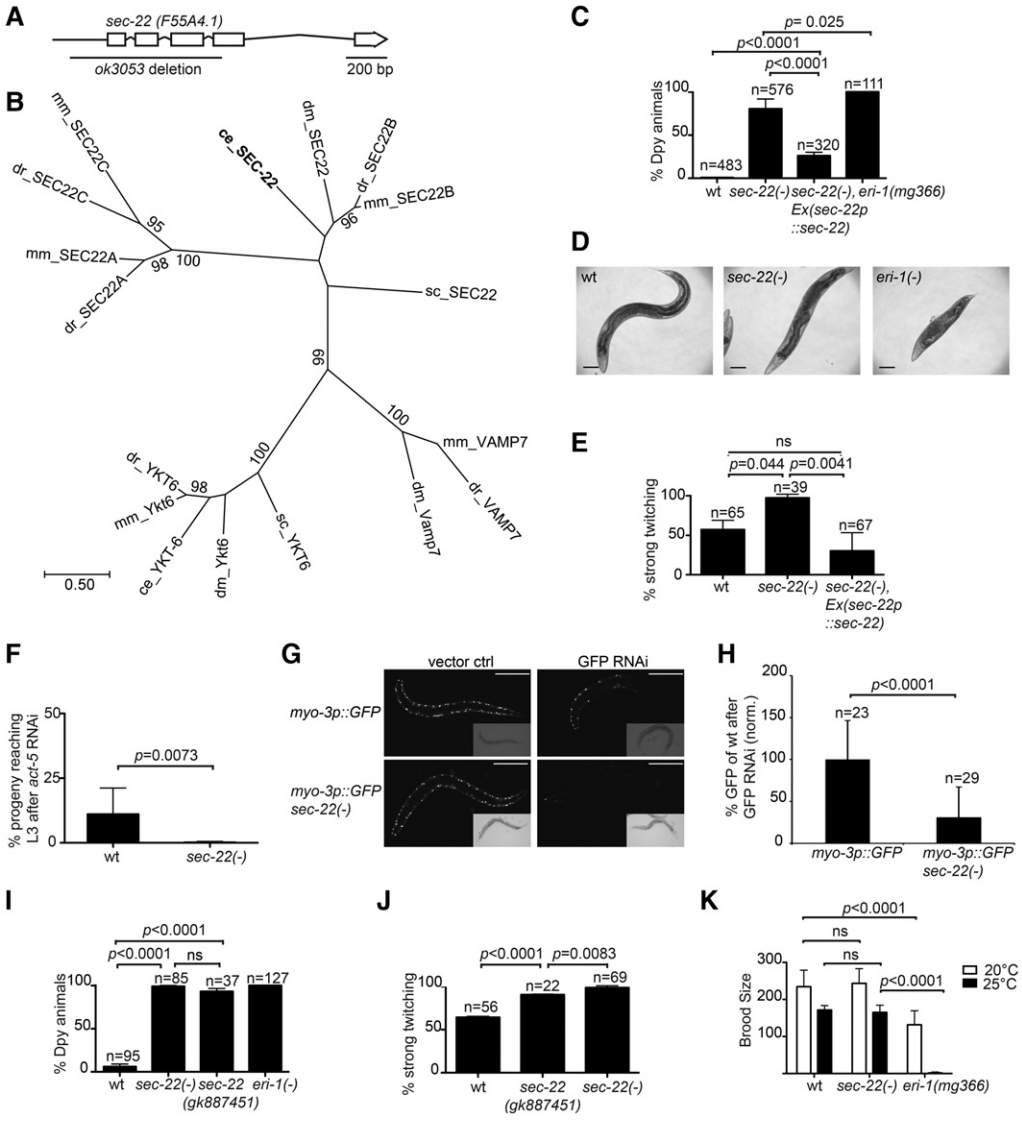

FIGURE 1. The SNARE SEC-22 inhibits RNAi in *C. elegans*. (*A*) Structure of the *sec-22/F55A4.1* gene. Sequence deleted in *sec-22(ok3053)* mutant [referred to as *sec-22(−)* in the following panels] indicated by solid line. (*B*) Phylogeny (using maximum likelihood method) of longin SNAREs from *Saccharomyces cerevisiae* (sc), *C. elegans* (ce), *Drosophila melanogaster* (dm), *Danio rerio* (dr), and *Mus musculus* (mm). Only positions with at least 95% coverage were used in the analysis. The tree is drawn to scale, with branch lengths measured in the number of substitutions per site. Bootstrap values of 75% or higher are indicated. Phylogenetic analyses were conducted using MEGA7 (Kumar et al. 2016). The multiple sequence alignment used in the phylogenetic analysis is shown in Supplemental Figure S1. (*C*) Percentage of affected (Dumpy) animals after bacteria-mediated (feeding) RNAi against the epidermis-expressed gene *dpy-13* in wild type (nine replicates), *sec-22(−)* mutant (10 replicates), *sec-22(−)* animals carrying an extrachromosomal array with a genomic *sec-22p::sec-22* fragment (10 replicates), and *eri-1(mg366)* mutant (three replicates). *n* = total number of animals. (*D*) Representative images of adult wild type, *sec-22(−)*, and *eri-1(mg366)* hermaphrodites after bacteria-mediated *dpy-13* RNAi. (*E*) Percentage of affected animals (strongly twitching in 2 mM levamisole) after feeding RNAi against the body wall muscle-expressed gene *unc-22* in wild type, *sec-22(−)* animals, and *sec-22(−)* animals carrying the extrachromosomal *sec-22p::sec-22* transgene. Data from three replicates; *n* = total number of animals. (*F*) Percentage survival for wild type and *sec-22(−)* animals after feeding RNAi against intestine-expressed gene *act-5*. Percentages were calculated from number of progeny developing past L3 larval stage compared to after L4440 vector control RNAi. Data for wild type and *sec-22(−)* from nine and 10 replicates, respectively. (*G*) Representative images of body wall muscle (bwm) GFP fluorescence (*myo-3p::GFP*) in wild type (*top*) and *sec-22(−)* animals (*bottom*) subjected to L4440 vector control feeding RNAi (*left*) or GFP RNAi (*right*). Anterior is to the *right*, scale bar 0.2 mm. (*H*) Quantification of GFP fluorescence as shown in panel *F*. Fluorescence after bacteria-mediated GFP RNAi was first normalized to the L4440 vector control and then to wild type (set to 100%). Data from three replicates; *n* = total number of animals analyzed. (*I*) Percentage of affected animals (Dpy) following feeding RNAi against epidermis-expressed gene *dpy-13* in wild type, *sec-22(−)* deletion mutant, *sec-22(gk887451)* mutant, and *eri-1(mg366)* mutant. Data from three replicates; *n* = total number of animals. (*J*) Percentage of affected animals (strongly twitching in levamisole) after feeding RNAi against body wall muscle-expressed gene *unc-22* in wild type (three replicates), *sec-22(gk887451)* (two replicates), and *sec-22(−)* (three replicates). *n* = total number of animals. (*K*) *sec-22(−)* mutants do not display temperature-dependent sterility. Brood sizes for wild type, *sec-22(−)*, and *eri-1(mg366)* animals grown at 20°C or 25°C, respectively. Data from three replicates for all strains and temperatures. Error bars indicate SD. Statistical analyses were carried out using one-way ANOVA and Tukey's test (for experiments with more than two groups, panels *C*, *E*, and *I*–*K*) or Student's *t*-test (for experiments with two groups, panels *F* and *H*).

enhanced RNAi phenotype associated with loss of *sec-22* is readily detected, it is not as strong as for many of the classical *eri* mutants, e.g., *eri-1(mg366)* (Fig. 1D; Kennedy et al. 2004). This may explain why *sec-22* has not been identified in previous forward genetic screens for mutants with enhanced RNAi (Simmer et al. 2002; Kennedy et al. 2004; Fischer et al. 2008; Pavelec et al. 2009).

Apart from the enhanced RNAi phenotype, the *sec-22(−)* mutant animals do not display any obvious phenotypes and their brood size at 20°C does not differ from wild type (Fig. 1K). However, additional phenotypes may appear only under specific conditions. For example, some mutants with enhanced RNAi, e.g., *eri-1*, display sterility as a result of defects in a specific endo-siRNA pathway, the 26G RNA pathway, causing deficient sperm development (Pavelec et al. 2009). For the *sec-22(−)* mutant, we found that the brood size at 25°C does not differ significantly from that of the wild-type strain, indicating that the 26G RNA pathway is functional (Fig. 1K).

SEC-22 primarily affects RNA import or cell autonomous RNAi

The observed enhanced RNAi in nonintestinal tissues (body wall muscle, epidermis) upon feeding RNAi of *sec-22* mutants could reflect alteration of any of several different steps. These include dsRNA uptake into intestinal cells, transport across the intestine, export into the extracellular space, import into the target tissue, or cell autonomous silencing of target gene expression. To investigate in which of these steps SEC-22 is required, we expressed SEC-22 from different tissue-specific promoters in the *sec-22(−)* mutant. If SEC-22 primarily inhibits uptake of environmental dsRNA into the intestine, or export from the intestine, expressing SEC-22 from an intestine-specific promoter should rescue the enhanced *unc-22* RNAi (body wall muscle) of the *sec-22(−)* mutant. In contrast, rescue of the enhanced *unc-22* RNAi phenotype by expression of SEC-22 only in the body wall muscle would indicate that SEC-22 functions in RNA import or cell autonomous RNAi. We found that expression of SEC-22 from the intestine-specific *sid-2* promoter (Winston et al. 2007) did result in a small but significant reduction of *unc-22* RNAi efficiency in response to feeding RNAi (Fig. 2A), supporting the former model. However, complete rescue was observed when SEC-22 was expressed using the body wall muscle-specific *myo-3* promoter (Fig. 2B). Moreover, this transgene suppressed RNAi to levels even lower than observed for the wild-type control (Fig. 2B). To assay whether overexpression of SEC-22 alone would inhibit RNAi, we introduced the *myo-3p::sec-22* transgene into wild-type animals. Indeed, the resulting transgenic animals displayed reduced RNAi in response to feeding RNAi against *unc-22* (Fig. 2C). Taken together, our data indicate that SEC-22 primarily inhibits import or cell autonomous RNAi in the target cell. However, we cannot at this point rule out an additional, minor role for SEC-22 in dsRNA uptake or transport across the intestine.

A rescuing mCherry::SEC-22 transgene is broadly expressed and colocalizes primarily with late endosomal proteins GFP::RAB-7 and LMP-1::GFP

To assay the expression and subcellular localization of the SEC-22 protein, we constructed a translational fluorescent mCherry::SEC-22 fusion protein driven by *sec-22* upstream sequence. The *sec-22p::mCherry::sec-22* transgene showed expression in most, if not all, somatic tissues (Fig. 3A–G). This is similar to the expression pattern of a previously reported transcriptional *sec-22p::*GFP fusion (Hunt-Newbury et al. 2007). It should be noted that the apparent lack of mCherry::SEC-22 expression in the germline is likely due to the strong suppression of multicopy transgenes in this tissue (Kelly et al. 1997). Importantly, we found that the mCherry::SEC-22 construct rescued the enhanced RNAi phenotype of the *sec-22(−)* mutant for both *dpy-13* and *unc-22* RNAi (Fig. 3H,I), indicating that the fusion protein is, at least in part, functional and correctly localized.

mCherry::SEC-22 appears concentrated to vesicular structures/punctae (Fig. 3). To determine the identity of

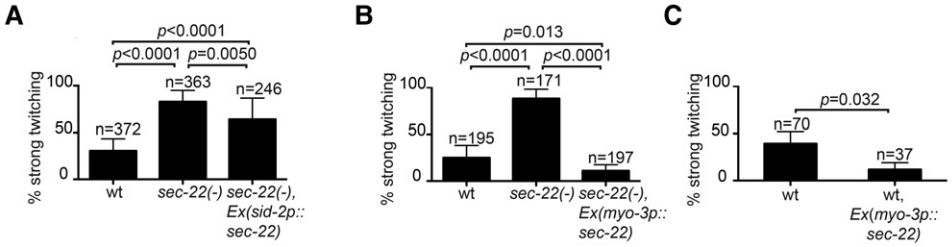

FIGURE 2. SEC-22 primarily inhibits cell autonomous RNAi or RNA import. (*A*) Percentage of affected animals after feeding RNAi targeting *unc-22* in wild-type, *sec-22(−)* animals, and *sec-22(−)* animals expressing *sec-22* in the intestine (*sid-2p::sec-22*). Data from 17 replicates; *n* = total number of animals. (*B*) Percentage of affected animals after *unc-22* feeding RNAi in wild-type, *sec-22(−)* animals, and *sec-22(−)* animals expressing *sec-22* in body wall muscle cells (*myo-3p::sec-22*). Data from 10 replicates; *n* = total number of animals. (*C*) Percentage of affected animals after feeding RNAi against *unc-22* in wild-type animals and wild-type animals transgenic for *sec-22* under the control of the body wall muscle *myo-3* promoter (*myo-3p::sec-22*). Data from three replicates; *n* = total number of animals. Error bars represent SD. Statistical analyses were carried out using one-way ANOVA followed by Tukey's test (for experiments with more than two groups, panels *A* and *B*) or Student's *t*-test (for experiments with two groups, panel *C*).

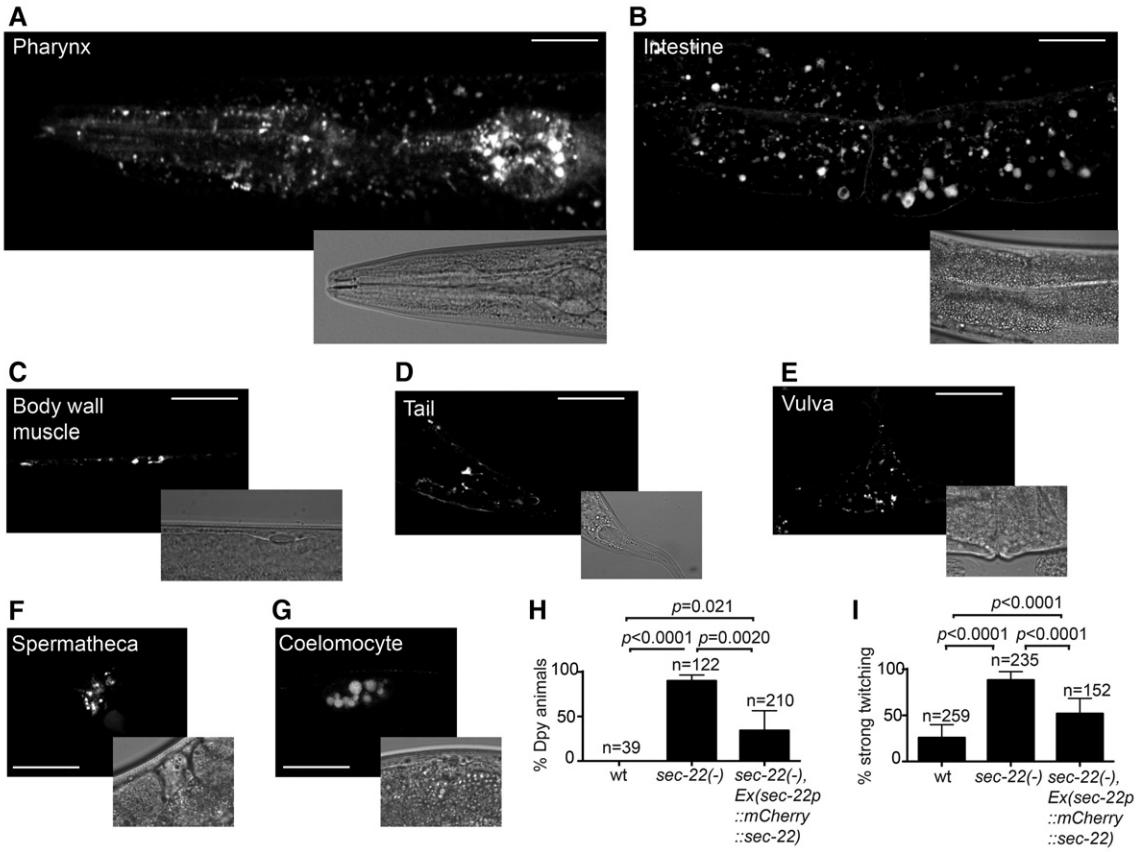

FIGURE 3. A rescuing mCherry::SEC-22 transgene is broadly expressed. Confocal fluorescence images of (*A*) pharynx, (*B*) intestine, (*C*) body wall muscle, (*D*) tail, (*E*) vulva, (*F*) spermatheca, and (*G*) coelomocyte from adult animals expressing an extrachromosomal *sec-22p::mCherry::sec-22* array. Scale bar, 20 µm for all images. (*H*) Percentage of affected animals (Dumpy) after *dpy-13* (epidermis) feeding RNAi in wild type, *sec-22(−)* mutant, and *sec-22(−)* mutant carrying the *sec-22p::mCherry::sec-22* extrachromosomal array. Data from three replicates, *n* = total number of animals. (*I*) Percentage of affected animals (strongly twitching in 2 mM levamisole) following feeding RNAi against body wall muscle-expressed gene *unc-22* in wild type, *sec-22(−)* mutant, and *sec-22(−)* mutant carrying the *sec-22p::mCherry::sec-22* extrachromosomal array. Data from 10 replicates; *n* = total number of animals. Error bars represent SD. All statistical analyses were carried out using one-way ANOVA followed by Tukey's test.

the mCherry::SEC-22 positive structures, we introduced GFP fusions of various proteins known to localize to specific intracellular membrane compartments (Treusch et al. 2004; Chen et al. 2006; Kang et al. 2007). Most of these GFP fusions are under the control of an intestine-specific promoter, and we therefore focused our investigations on the intestine. We found that mCherry::SEC-22 colocalized significantly (object colocalization) with the late endosomal/lysosomal markers GFP::RAB-7 (Fig. 4A,D) and LMP-1::GFP (Fig. 4B, D) but not with acidified lysosomes marked by LysoTracker Green (Fig. 4C,D), Golgi (mans::GFP), early endosomes (GFP::RAB-5), autophagosomes (LGG-1::GFP), or recycling endosomes (GFP::RAB-11) (Fig. 4D; Supplemental Fig. S2). GFP::RAB-7 and LMP-1::GFP partially localize to acidified late endosomes/lysosomes (Treusch et al. 2004; Chen et al. 2006; Chotard et al. 2010). However, the lack of LysoTracker Green staining of mCherry::SEC-22-positive vesicles indicates that these primarily represent nonacidified late endosomes. Notably, despite the lack of colocalization between mCherry::SEC-22 and markers other than GFP::RAB-7 and LMP-1::GFP, the overlap with the late endosomal markers is not complete (Fig. 4A,B,D). This indicates that additional compartments labeled by mCherry::SEC-22 remain to be identified. GFP::RAB-7 and LMP-1::GFP appeared to localize to the limiting membrane of the vesicles, and although membrane-localized mCherry::SEC-22 could be observed, this fusion protein primarily localized inside the GFP::RAB-7 and LMP-1::GFP-positive vesicles (Fig. 4A,B). The reason for the predominantly intralumenal mCherry::SEC-22 localization is presently not known, but a possible explanation is that after formation of *trans*-SNARE complexes and vesicle fusion, membrane-localized mCherry::SEC-22 is packaged into intralumenal vesicles (ILVs) of late endosomes/MVBs for lysosomal degradation. Alternatively, mCherry::SEC-22 containing ILVs may be exported out of the cell by fusion of the late endosomes/MVBs to the plasma membrane.

We previously showed that endogenous SID-5 can be detected by immunostaining (Hinas et al. 2012). Unfortunately, the mCherry::SEC-22 fluorescence is relatively weak, and we have therefore, despite our best efforts, failed to identify

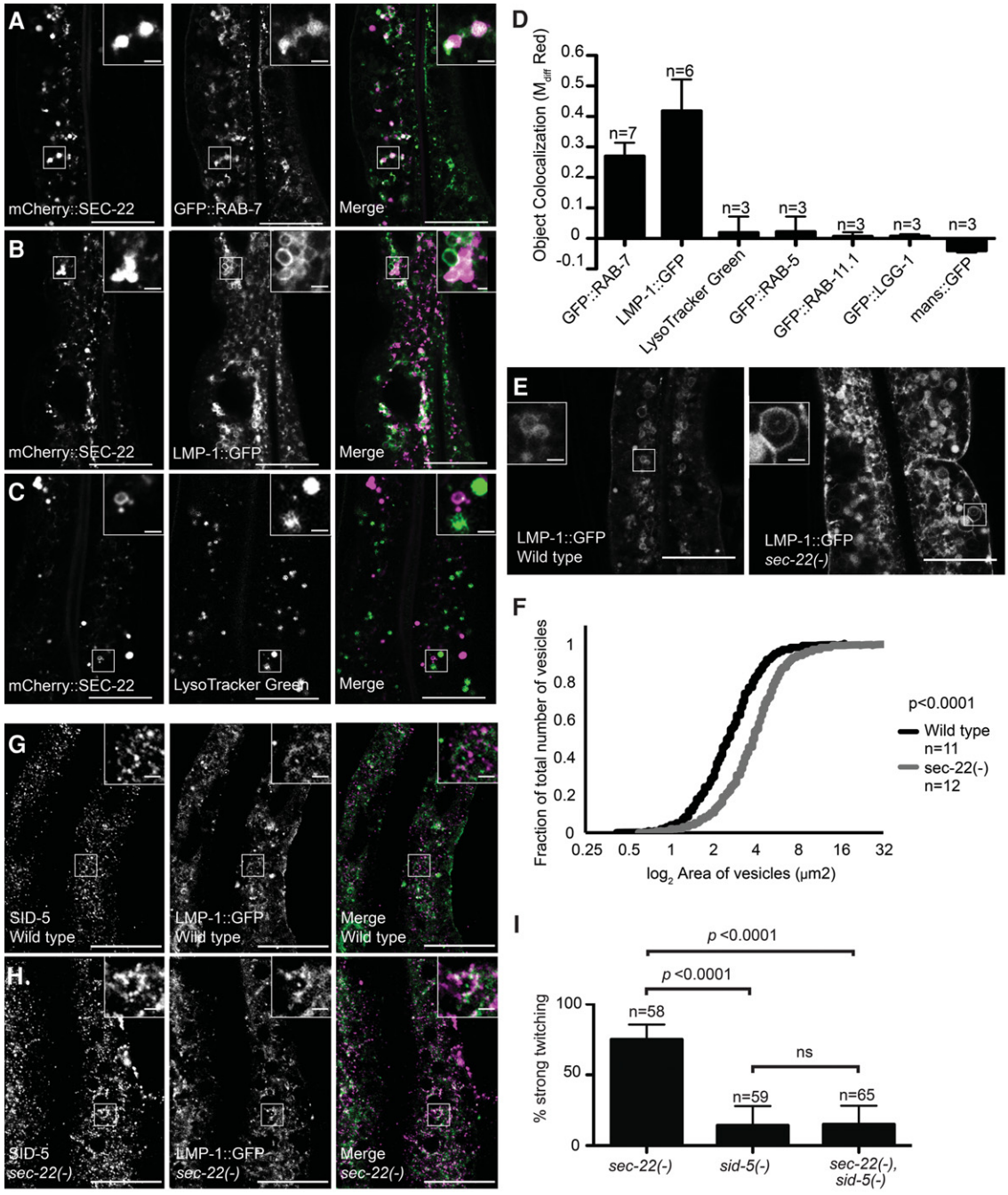

FIGURE 4. mCherry::SEC-22 colocalizes with late endosomal proteins GFP::RAB-7 and LMP-1::GFP, and loss of *sec-22* results in enlarged LMP-1::GFP positive vesicles. Confocal fluorescence imaging of intestinal cells (int2) in adult animals expressing the extrachromosomal *sec-22p::mCherry::sec-22* array (*left*) in combination with GFP::RAB-7 (*center*, *A*), LMP-1::GFP (*center*, *B*), or with LysoTracker Green staining (*center*, *C*). (*Right*) Merge with mCherry pseudocolored in magenta and GFP/LysoTracker Green pseudocolored in green. Scale bar 20 µm; *insets*, 2 µm. The apparent lack of mCherry fluorescence in some intestinal cells is most likely due to mosaicity of the transgenic *sec-22p::mCherry::sec-22* extrachromosomal array. (*D*) Quantification of object colocalization in images represented in *A–C* and Supplemental Figure S2 in fraction of mCherry::SEC-22 objects colocalizing with GFP/LysoTracker Green objects, the contribution from independent colocalization subtracted ($M_{Diff\ Red}$). Error bars represent SD. (*E*) Confocal imaging of LMP-1::GFP expression in intestinal cells (int2) from wild-type (*left*) and *sec-22(−)* (*right*) animals. Scale bar 20 µm; *insets*, 2 µm. Additional representative images can be found in Supplemental Figure S3. (*F*) Cumulative plots of LMP-1::GFP vesicle size in wild-type and *sec-22(−)* animals. *n* = number of animals. For each animal, 3–4 images were analyzed, for a total of 1700 vesicles per strain. For more details on quantification, see Materials and Methods. (*G,H*) Immunostaining of dissected intestines using a polyclonal SID-5 antiserum in wild type (*G*) or *sec-22(−)* (*H*) strains expressing LMP-1::GFP. (*Left*) SID-5, (*center*) LMP-1::GFP, (*right*) merge of SID-5 (pseudocolored in magenta) and LMP-1::GFP (pseudocolored in green). Scale bar 20 µm; *insets*, 2 µm. (*I*) Percentage of affected animals following *unc-22* feeding RNAi in *sec-22(−)* and *sid-5(−)* single mutants and in *sec-22(−) sid-5(−)* double mutant animals. Data from three replicates; *n* = total number of animals. Error bars represent SD. Statistical analysis in *I* was carried out using one-way ANOVA followed by Tukey's test.

immunostaining conditions where SID-5 and mCherry::SEC-22 can be visualized simultaneously. Furthermore, fusing SID-5 to GFP results in a nonrescuing transgene that even acts as a dominant negative, and SID-5::GFP localization may therefore not reflect endogenous SID-5 localization (Hinas et al. 2012). Despite the present lack of colocalization data for SID-5 and SEC-22, it is interesting to note that endogenous SID-5, like mCherry::SEC-22, associates primarily with late endosome markers GFP::RAB-7 and LMP-1::GFP (Hinas et al. 2012).

Loss of SEC-22 results in enlarged late endosomes

Late endosomes/MVBs are known to fuse with lysosomes, leading to degradation of the contents. Furthermore, late endosomes/MVBs are important for RNAi and miRNA silencing activity in mammals and *D. melanogaster* (Gibbings et al. 2009; Lee et al. 2009; Harris et al. 2011). Since SEC-22 is a SNARE and we found that it localizes to late endosomes/MVBs, we hypothesized that it may function in fusion between late endosomes/MVBs and lysosomes, directly or indirectly. Supporting this hypothesis, we found that *sec-22(−)* animals have significantly larger LMP-1::GFP positive vesicles compared to wild type (Fig. 4E,F; Supplemental Fig. S3). In a recent study, enlarged late endosomes were observed in *D. melanogaster Sec22* mutants and were suggested to result from defective ER–Golgi transport (Zhao et al. 2015). Although more experiments are required to fully rule out a similar explanation for our observations, the mCherry::SEC-22 colocalization with late endosomes indicates that, at least in *C. elegans*, SEC-22 affects late endosome size in a more direct manner.

sec-22 regulates RNAi in a *sid-5*-dependent manner

In wild-type *C. elegans*, SID-5 is detected in cytoplasmic foci that often surround late endosomes (Hinas et al. 2012). To investigate whether SID-5 requires SEC-22 to associate with late endosomes, we carried out immunostaining of SID-5 in a strain expressing LMP-1::GFP in a wild type or *sec-22 (−)* background, respectively (Fig. 4G,H). This experiment showed that despite loss of *sec-22*, SID-5 positive vesicular structures are able to associate with the enlarged LMP-1::GFP-positive vesicles. The observation that SID-5 localizes to late endosomes also in *sec-22(−)* mutant animals is consistent with several alternative models. Most importantly, it does not differ between a model where *sec-22* depends on *sid-5* and a model where the opposite is true. To gain further insight into the genetic relationship between *sid-5* and *sec-22*, we therefore constructed a *sec-22(−) sid-5(−)* double mutant. The *sec-22(−) sid-5(−)* mutant was subjected to feeding RNAi against the body wall muscle target *unc-22* (Fig. 4H). This demonstrated that *sid-5* is epistatic to *sec-22* as the RNAi efficiency of the *sec-22(−) sid-5(−)* double mutant did not significantly differ from that of the *sid-5(−)* single mutant. Thus, *sec-22* requires *sid-5* to regulate RNAi. For example, SEC-22 may promote lysosomal degradation of SID-5 or otherwise inhibit SID-5, thus reducing RNAi efficiency.

In the simplest model, SEC-22 resides in the outer membrane of late endosomes and promotes fusion to lysosomes by forming a *trans*-SNARE complex with lysosomal SNAREs, leading to degradation of imported RNAi silencing signals and/or associated proteins, which may include SID-5. In addition, several alternative mechanisms of function are possible. For example, SEC-22 may initially reside in transport vesicles and interact with late endosome SNAREs, thereby delivering factors to late endosomes that in turn promote fusion to lysosomes. This would be similar to the function of mouse Sec22b in delivery of ER proteins to phagosomes via ERGIC vesicles in dendritic cells (Cebrian et al. 2011). Interestingly, SID-5 is detected in small vesicle-like structures (Hinas et al. 2012, and this study), which may represent such transport vesicles. In addition to the effect of late endosomes/MVBs on RNAi and miRNA silencing, autophagy has been shown to inhibit miRNA silencing in mammals as well as in *C. elegans* (Gibbings et al. 2012; Zhang and Zhang 2013). However, the strong colocalization of mCherry::SEC-22 with late endosomes/MVBs and the lack of colocalization with autophagosomes suggest that the function of SEC-22 in RNAi is related to late endosomes/MVBs rather than to autophagy. Furthermore, although the 26G RNA appears unaffected in the *sec-22(−)* mutant, other endogenous small RNA pathways may be altered. This may in turn leave more shared factors available for the exogenous RNAi pathway, resulting in the observed enhanced RNAi, as described previously for other mutants (Lee et al. 2006). More experiments are required to distinguish between these and other possible models.

From our tissue-specific rescue experiments, we found that SEC-22 primarily affects RNAi in the target tissue, but that it may additionally affect dsRNA uptake into the intestine or export to other tissues. Importantly, late endosomes/MVBs are also the source of exosomes, extracellular vesicles that have been suggested to carry RNA between cells (Valadi et al. 2007; Patton et al. 2015). It is thus possible that loss of SEC-22 also leads to an increase in RNA export from the intestine. Interestingly, SID-5 has been suggested to promote RNA export (Hinas et al. 2012). The finding that the enhanced RNAi phenotype of *sec-22(−)* mutant animals requires SID-5 further supports this hypothesis. However, SID-5 appears dispensable in the target tissue (Hinas et al. 2012), indicating that SEC-22 also acts through other proteins. Many questions remain and additional studies will be needed to pinpoint the exact mechanism of the functions of SEC-22 and SID-5 in membrane trafficking and RNAi. Nevertheless, our findings provide evidence for a noncanonical function of the classical ER–Golgi SNARE SEC-22 in RNAi. It will be most interesting to investigate whether SEC-22 homologs in other organisms similarly modulate RNAi efficiency.

MATERIALS AND METHODS

C. elegans maintenance and strains used in the study

All *C. elegans* strains were maintained at 20°C on *E. coli* strain OP50 grown on standard NGM plates unless stated otherwise (Brenner 1974).

The *sec-22(ok3053)* strain obtained from the National Bioresource Project, Japan, was outcrossed six times before further analysis (outcrossed strain was named AHS10). Strains used in the study were wild-type Bristol strain N2 (Brenner 1974), RB2256 *sec-22 (ok3053) X*, AHS10 *sec-22(ok3053) X* (outcrossed 6x), GR1373 *eri-1(mg366) IV*, AHS18 *ccIs4251[myo-3::GFP*[1]*] I; sec-22(ok3053) X*, AHS30 *sec-22(ok3053) dpy-8 (e130) sid-5(qt24) X*, AHS36 *ccIs4251 [myo-3::GFP*[1]*] I*, AHS42 *sec-22(ok3053) X; uppEx14[sec-22p::sec-22; myo-3p::DsRed2]*, AHS51 *sec-22(ok3053) X; uppEx16[myo-3p::sec-22; myo-3p::DsRed2]*, AHS53 *sec-22(ok3053) X; uppEx18[sec-22p::mCherry::sec-22]*, AHS54 *ccIs4251[myo-3::GFP*[1]*] I; uppEx33 [myo-3p::sec-22; myo-3p::DsRed2]*, AHS59 *sec-22(ok3053) X; uppEx20[sid-2p::sec-22; sid-2p::DsRed2]*, RT258 *unc-119(ed3) III; pwIs50[lmp-1::GFP + Cb-unc-119(+)]* (Treusch et al. 2004), RT476 *unc-119(ed3) III; pwIs170[vha-6p::GFP::rab-7 + Cb unc-119 (+)]* (Chen et al. 2006), RT327 *unc-119(ed3) III; pwIs72[vha-6p::GFP::rab-5 + unc-119(+)]* (Chen et al. 2006), RT1315 *unc-119 (ed3) III; pwIs503[vha-6p::mans::GFP + Cb-unc-119(+)]*(29), RT311 *unc-119(ed3) III; pwIs69[vha6p::GFP::rab-11 + unc-119(+)]* (Chen et al. 2006), DA2123 *adIs2122[lgg-1::GFP + rol-6(su1006)]* (Kang et al. 2007), AHS61 *adIs2122[lgg-1::GFP + rol-6(su1006)]; uppEx18[sec-22p::mcherry::sec-22]*, AHS62 *pwIs69[vha6p::GFP::rab-11 + unc-119(+)]; uppEx18[sec-22p::mcherry::sec-22]*, AHS63 *pwIs503[vha-6p::mans::GFP + Cb-unc-119(+)]; uppEx18[sec-22p::mcherry::sec-22]*, AHS64 *pwIs72[vha-6p::GFP::rab-5 + unc-119(+)]; uppEx18[sec-22p::mcherry::sec-22]*, AHS65 *pwIs170[vha-6p::GFP::rab-7 + Cb unc-119(+)]; uppEx18[sec-22p::mcherry::sec-22]*, AHS66 *pwIs50[lmp-1::GFP + Cb-unc-119(+)]; uppEx18[sec-22p::mcherry::sec-22]*, AHS83 *sec-22(ok3053) X; pwIs50[lmp-1::GFP + Cb-unc-119(+)]*, and VC40930 *sec-22(gk887451)*. All new strains were obtained by standard genetic crosses or by microinjection (see Transgenes section below).

Brood size assay

For brood size assays (Fig. 1K), L4 hermaphrodites were placed on OP50-seeded NGM plates and grown at 20°C and 25°C, respectively. The hermaphrodites were moved to new seeded plates every day until no larvae could be found on the plate. The number of progeny was counted when they had reached the L4 larval stage. The brood size of each hermaphrodite represents the total number of progeny.

Yeast two-hybrid screen

The yeast two-hybrid screen was carried out using the Dualmembrane system (Stagljar et al. 1998) (DualSystemsBiotech) according to the manufacturer's instructions. Briefly, total RNA was prepared from mixed stage *C. elegans* using TRIzol extraction (Invitrogen). After chloroform extraction, isopropanol precipitation, and DNase treatment (TURBO DNA-free kit, Ambion), the RNA was used as template for cDNA synthesis. *sid-5* cDNA was reverse transcribed using SuperScript II (Invitrogen) and primer sid-5 bait y2h rev 2 (5′-ATTCTAGAGGCCGAGGCGGCCGCGT-CTCTAATTCCGATGATTGGC-3′). Amplification of the *sid-5* sequence and addition of SfiI restriction sites were achieved by PCR using the Advantage PCR kit (Clontech) and primers sid-5 bait y2h forw 2 (5′-ATTCTAGAGGCCATTACGGCCATGCCCAGCAAAAACTGTGCCAAA-3′) and sid-5 bait y2h rev 2. After gel purification, the *sid-5* fragment was cloned into a TOPO vector (Invitrogen) and sequence verified. The *sid-5* fragment was then excised using SfiI, cloned into the pBT3-SUC vector, and transformed into the *S. cerevisiae* NMY51 strain (DualSystemsBiotech).

The prey cDNA library was constructed using the SMART cDNA library kit (Clontech). Briefly, 1 µg DNase-treated *C. elegans* total RNA was used for first strand cDNA synthesis using oligo CDS III/3′ [5′-ATTCTAGAGGCCGAGGCGGCCGACATG-dT(30)N_{-1}N-3′, where N = A, G, C, or T; N_{-1} = A, G, or C]. The cDNA was then amplified by long-distance PCR followed by SfiI digestion, CHROMA SPIN-400 column purification, and ethanol precipitation. For amplification of the cDNA library, the SfiI-digested DNA (200 ng) was ligated into the pPR3-N prey vector (500 ng) and transformed into electrocompetent DH10B *E. coli* cells (Invitrogen). After plasmid preparation, 7 µg was transformed into NMY51 expressing pBT3-SUC/sid-5 and the transformed cells were plated on SD-AHLW (synthetic defined medium lacking adenine, histidine, leucine, and tryptophan) plates supplemented with 2.5 mM 3-amino-1,2,4-triazole (3-AT). When colonies appeared after 4 d of incubation, β-galactosidase activity was assayed. Plasmids were extracted from positive clones and retransformed for confirmation prior to sequencing of the inserts. Out of 127 sequenced clones, two represented *F55A4.1/sec-22*. Retransformation of one of these clones together with the pBT3-SUC/sid-5 vector resulted in 344 colonies, compared to 234 colonies after cotransformation with the negative control bait plasmid pCCW/Alg5.

Transgenes

All constructs were microinjected into *C. elegans* as described previously (Mello et al. 1991).

The *sec-22p::sec-22* fragment was PCR amplified from genomic DNA using primers F55A4.1 upstream3 (5′- CTTCTCTTGCAGGGCAATTGA-3′) and sec-22 3′UTR rev (5′-GATAAAGCATGTTCTGCCCCT-3′). The resulting product (5 ng/µL) was coinjected with *myo-3p::DsRed2* (pHC183) plasmid (25 ng/µL; Winston et al. 2002) into strain AHS10 and a representative line was designated AHS42.

The *sid-2p::sec-22* construct was obtained by PCR stitching (Hobert 2002). The *sid-2* promoter was amplified from genomic DNA using primers sid2p for (5′-CTGCCTATTGGGACTCAACG-3′) and sid2psec22 rev (5′-GGCAATTAGCGTTAGCTCCATTTCCTGAAAATATCAGGGTTTTG-3′), and the *sec-22* coding and downstream sequence was amplified from genomic DNA using primers sid2psec22 for (5′-CAAAACCCTGATATTTTCAGGAAATGGAGCTAACGCTAATTGCC-3′) and sec22 rev (5′-GTCCACCAATCCAGGCTTTA-3′). The two fragments were then joined by PCR using primers sid-2p for and sec-22 rev. For the coinjection marker *sid-2p::DsRed2,* the *sid-2p* fragment was amplified from genomic DNA using primers sid2p for and sid-2pDsRed rev (5′-CG

[1]Complete *myo-3::GFP* genotype is ccIs4251[pSAK2 (myo-3 promoter driving a nuclear-targeted GFP-LacZ fusion), pSAK4 (myo-3 promoter driving mitochondrially targeted GFP) and a dpy-20 subclone] I (Winston et al. 2002).

TTCTCGGAGGAGGCCATTTCCTGAAAATATCAGGGTTTTG -3′), and the *DsRed2* fragment was amplified from plasmid pHC183 (Winston et al. 2002) using primers sid-2pDsRed for (5′-CAAAA CCCTGATATTTTCAGGAAATGGCCTCCTCCGAGAACG-3′) and DsRed rev (5′- CGGTCATAAACTGAAACGTAAC-3′). The resulting fragments were then joined by PCR using primers sid-2p for and DsRed rev. The *sid-2p::sec-22* (5 ng/μL) and the *sid-2p::DsRed2* (25 ng/μL) fragments were then coinjected into the AHS10 strain and a representative line was designated AHS59.

For the *myo-3p::sec-22* transgene, the *myo-3p* fragment was constructed by PCR amplification from plasmid pHC183 (Winston et al. 2002) using primers myo3p for (5′-GGCTGAAATCACT CACAACGATGG -3′) and myo3psec22 rev (5′- GGCAATTAGCG TTAGCTCCAT-AAATTAGACGGTAAAAGT-3′). The *sec-22* coding and downstream sequence was amplified from genomic DNA using primers myo3sec22 for (5′-ACTTTTACCGTCTAATTT-A TGGAGCTAACGCTAATTGCC-3′) and sec22 rev (5′-GTCCACC AATCCAGGCTTTA-3′). The *myo-3p* (4.8 ng/μL) and *sec-22* (2.5 ng/μL) fragments were injected to be fused in vivo, together with *myo-3p::DsRed2* (pHC183) plasmid (25 ng/μL; Winston et al. 2002). A representative line was designated AHS51.

For construction of *sec-22p::mCherry::sec-22*, the upstream sequence was amplified from genomic DNA using primers sec-22p for (5′-CTGTGTTCTCTTCTCTTGCA-3′) and sec-22p rev (5′-C TTCTTCACCCTTTGAGACCAT-TACTCTGAAAATAAAAACTT AATAG-3′). *mCherry* was amplified using plasmid pCFJ90 (from the E. Jorgensen laboratory) as template and primers mCherry for (5′-ATGGTCTCAAAGGGTGAAGAAG-3′) and mCherry rev (5′- CTTATACAATTCATCCATGCCA-3′). The coding and downstream region of *sec-22* was amplified from genomic DNA using oligonucleotides sec-22 end (5′-TGGCATGGATGAATTGTATAA G-ATGGAGCTAACGCTAATTGCC-3′) and sec-22 3′UTR rev (5′-GATAAAGCATGTTCTGCCCCT-3′). The fragments were then joined by PCR using primers sec-22p for and sec-22 3′UTR rev. The *sec-22p::mCherry::sec-22* construct (30 ng/μL) was injected into strain AHS10 and a representative line was designated AHS53.

RNAi

Bacteria-mediated RNAi was carried out essentially as described previously (Timmons et al. 2001). For RNAi constructs with dual T7 promoters (*unc-22*, *dpy-13,* and *act-5*) (Kamath et al. 2003), L4 hermaphrodites were placed on bacteria grown for 24 h on NGM plates supplemented with 50 μg/mL carbenicillin and 1 mM IPTG. Phenotypes were scored when the progeny had reached adulthood. For *unc-22* RNAi, only strong, continuous whole-body twitching within 10 sec in 2 mM levamisole in M9 buffer was scored as positive. For *act*-5 RNAi, the number of progeny surviving at least to the L3 larval stage was scored. For GFP feeding RNAi, bacteria expressing a *GFP* hairpin were prepared as described in Winston et al. (2002).

LysoTracker Green staining

L4 hermaphrodites were placed on OP50 seeded NGM plates with 100 nM LysoTracker Green DND-26 (Life Technologies) and left to mature to gravid adults overnight at 20°C before image acquisition.

Microscopy

For quantification of GFP expression (Fig. 1G,H), worms in L4 or young adult stage were harvested from 5 cm NGM plates by rinsing the plates with 800 μL M9/0.1% Tween-20 solution, and transferring the worms in suspension to 1.5 mL eppendorff tubes where they sunk to the bottom. Excess M9 solution was carefully removed and 10 μL 2 mM levamisole was added. Within a few seconds, paralyzed worms were transferred to 2% agarose pads on microscope slides by micropipette and a cover slip was applied. Worms were then imaged using a Nikon eclipse 90i microscope with a 2× Plan Apochromat objective, in both FITC and brightfield channels.

Fluorescence microscopy images of mCherry::SEC-22 and GFP fusion proteins as well as SID-5 immunostaining (Figs. 3, 4; Supplemental Figs. S2, S3) were obtained using a Zeiss LSM710 confocal microscope and the standard Zeiss Zen software. SID-5 immunohistochemistry of dissected *C. elegans* intestines was carried out using a rabbit polyclonal primary antibody as previously described (Hinas et al. 2012), except that the secondary antibody was an Alexa Fluor 555-conjugated donkey anti-rabbit antibody (Invitrogen). For microscopy of nonfixed animals, adult hermaphrodites (1 d post L4 stage) were mounted on 2% agarose pads and paralyzed using 2 mM levamisole. Microscope settings were selected using the smart setup function, optimizing for best signal. The following excitation laser wavelengths were used: autofluorescent material (gut granules), 405 nm; mCherry and Alexa Fluor 555, 555 nm; and GFP, 488 nm.

Quantification of body wall muscle GFP

For image analysis and quantification of body wall muscle GFP fluorescence (Fig. 1G), CellProfiler 2.0.0 (version rev dc7da2e) was used (Carpenter et al. 2006; Wählby et al. 2012). Worms were identified using the IdentifyPrimaryObjects module using the RobustBackground Global thresholding method, with a threshold correction factor of 1.05. In order to segment worms adjacent to each other that were identified as a single object by the previous algorithm, the Untangle Worms module was used, with a custom-generated training set. Identified objects were then manually controlled and corrected if needed. In order to quantify the effect of silencing on GFP expression, the number of body wall muscle nuclei with a GFP signal above a certain threshold was counted per worm. GFP-positive nuclei were identified using the IdentifyPrimaryObjects module, using the manual thresholding method and a manual threshold of 0.05. To distinguish clumped objects, the Laplacian of Gaussian method was used with the threshold automatically calculated using the Otsu method, LoG filter diameter 2.0, smoothing filter set to 0, and a 2 pixel minimum allowed distance for local maxima. The nuclei identified in this step were subsequently related to the previously identified worms and the number of GFP-positive nuclei per worm was exported as comma-separated values.

Quantification of colocalization

Image analysis for quantification of colocalization (Fig. 4D) was done using a collection of custom ImageJ macros. To avoid issues with heterogeneous expression, all channels were contrast-adjusted so that 0.4% pixels were saturated. Since only the vesicular fraction

of the GFP-fused marker proteins was of interest, the GFP channel was treated as follows, so that vesicles and punctate structures were enhanced. A median filter was applied with a radius of 20 pixels. Segmentation was performed by intensity thresholding. The binary image was despeckled to remove noise and objects with an area of less than three pixels were filtered. This treatment was sufficient to detect all punctae and most vesicles. The mCherry channel was treated with ImageJ's rolling circle background subtraction algorithm, using a radius of 30, and a smoothing filter. A manual threshold was used to produce a binary image followed by a Despeckle operation.

Colocalization was represented by Manders' coefficients (Manders et al. 1993): two values per image: the ratios of total colocalization between the red and green channels, and the total area of red and green channels, respectively (M_{Red} and M_{Green}). A Region of Interest was set for each image, including only cells with mCherry::SEC-22 expression and excluding intestinal lumen and nucleus. For significance estimation, 100 randomized images were generated from the source images to simulate a null hypothesis of no correlation. This was done by scrambling the positions of the detected objects within the region of interest in the mCherry channel. Manders' coefficients were calculated as above from the scrambled images and $M_{\text{Diff Red}}$ and $M_{\text{Diff Green}}$ values were calculated by subtracting the median $M_{\text{Red Scramble}}$ and $M_{\text{Green Scramble}}$ from the original images. Significance was calculated by paired (M_{Red} vs median $M_{\text{Red Scramble}}$) two-tailed heteroscedastic Student's *t*-test.

Quantification of LMP-1::GFP vesicle size

Vesicle area sizes were measured manually in ImageJ by marking them as regions of interest. Image file names were obfuscated to ensure unbiased scoring. All measured vesicle areas were pooled, and the difference in area size between strains was tested for significance using the two-sample Kolmogorov–Smirnov test.

SUPPLEMENTAL MATERIAL

Supplemental material is available for this article.

ACKNOWLEDGMENTS

The authors are grateful to F. Söderbom, C. Hunter, G. Wagner, and D. Li for discussions and critical reading of the manuscript and to L. Klasson for input on phylogenetic analysis. *C. elegans* strains were provided by the National BioResource Project (NBRP), Japan, as well as by the CGC, which is funded by National Institutes of Health Office of Research Infrastructure Programs (P40 OD010440). This study was funded by grants from the Wenner-Gren Foundations (Wenner-Gren Fellow), Swedish Foundation for Strategic Research, Swedish Research Council, Ake Wiberg's Foundation, and Carl Trygger's Foundation (to A.H.).

Received July 27, 2016; accepted December 9, 2016.

REFERENCES

Barlowe CK, Miller EA. 2013. Secretory protein biogenesis and traffic in the early secretory pathway. *Genetics* **193:** 383–410.

Brenner S. 1974. The genetics of *Caenorhabditis elegans*. *Genetics* **77:** 71–94.

Carpenter AE, Jones TR, Lamprecht MR, Clarke C, Kang IH, Friman O, Guertin D, Chang JH, Lindquist R, Moffat J, et al. 2006. CellProfiler: image analysis software for identifying and quantifying cell phenotypes. *Genome Biol* **7:** R100.

Cebrian I, Visentin G, Blanchard N, Jouve M, Bobard A, Moita C, Enninga J, Moita LF, Amigorena S, Savina A. 2011. Sec22b regulates phagosomal maturation and antigen crosspresentation by dendritic cells. *Cell* **147:** 1355–1368.

Chen CCH, Schweinsberg PJ, Vashist S, Mareiniss DP, Lambie EJ, Grant BD. 2006. RAB-10 is required for endocytic recycling in the *Caenorhabditis elegans* intestine. *Mol Biol Cell* **17:** 1286–1297.

Chotard L, Mishra AK, Sylvain MA, Tuck S, Lambright DG, Rocheleau CE. 2010. TBC-2 regulates RAB-5/RAB-7-mediated endosomal trafficking in *Caenorhabditis elegans*. *Mol Biol Cell* **21:** 2285–2296.

Cikaluk DE, Tahbaz N, Hendricks LC, DiMattia GE, Hansen D, Pilgrim D, Hobman TC. 1999. GERp95, a membrane-associated protein that belongs to a family of proteins involved in stem cell differentiation. *Mol Biol Cell* **10:** 3357–3372.

Filippini F, Rossi V, Galli T, Budillon A, D'Urso M, D'Esposito M. 2001. Longins: a new evolutionary conserved VAMP family sharing a novel SNARE domain. *Trends Biochem Sci* **26:** 407–409.

Fire A, Xu S, Montgomery MK, Kostas SA, Driver SE, Mello CC. 1998. Potent and specific genetic interference by double-stranded RNA in *Caenorhabditis elegans*. *Nature* **391:** 806–811.

Fischer SEJ, Butler MD, Pan Q, Ruvkun G. 2008. *Trans*-splicing in *C. elegans* generates the negative RNAi regulator ERI-6/7. *Nature* **455:** 491–496.

Ghildiyal M, Zamore PD. 2009. Small silencing RNAs: an expanding universe. *Nat Rev Genet* **10:** 94–108.

Gibbings DJ, Ciaudo C, Erhardt M, Voinnet O. 2009. Multivesicular bodies associate with components of miRNA effector complexes and modulate miRNA activity. *Nat Cell Biol* **11:** 1143–1149.

Gibbings D, Mostowy S, Jay F, Schwab Y, Cossart P, Voinnet O. 2012. Selective autophagy degrades DICER and AGO2 and regulates miRNA activity. *Nat Cell Biol* **14:** 1314–1321.

Hamamichi S, Rivas RN, Knight AL, Cao S, Caldwell K, Caldwell G. 2008. Hypothesis-based RNAi screening identifies neuroprotective genes in a Parkinson's disease model. *Proc Natl Acad Sci* **105:** 728–733.

Harris DA, Kim K, Nakahara K, Vásquez-Doorman C, Carthew RW. 2011. Cargo sorting to lysosome-related organelles regulates siRNA-mediated gene silencing. *J Cell Biol* **194:** 77–87.

Hinas A, Wright AJ, Hunter CP. 2012. SID-5 is an endosome-associated protein required for efficient systemic RNAi in *C. elegans*. *Curr Biol* **22:** 1938–1943.

Hobert O. 2002. PCR fusion-based approach to create reporter gene constructs for expression analysis in transgenic *C. elegans*. *Biotechniques* **32:** 728–730.

Hunt-Newbury R, Viveiros R, Johnsen R, Mah A, Anastas D, Fang L, Halfnight E, Lee D, Lin J, Lorch A, et al. 2007. High-throughput in vivo analysis of gene expression in *Caenorhabditis elegans*. *PLoS Biol* **5:** 1981–1997.

Jose AM, Kim Y, Leal-Ekman S, Hunter CP. 2012. Conserved tyrosine kinase promotes the import of silencing RNA into *Caenorhabditis elegans* cells. *Proc Natl Acad Sci* **109:** 14520–14525.

Kamath RS, Fraser AG, Dong Y, Poulin G, Durbin R, Gotta M, Kanapin A, Le Bot N, Moreno S, Sohrmann M, et al. 2003. Systematic functional analysis of the *Caenorhabditis elegans* genome using RNAi. *Nature* **421:** 231–237.

Kang C, You NJ, Avery L. 2007. Dual roles of autophagy in the survival of *Caenorhabditis elegans* during starvation. *Genes Dev* **21:** 2161–2171.

Kelly WG, Xu S, Montgomery MK, Fire A. 1997. Distinct requirements for somatic and germline expression of a generally expressed *Caenorhabditis elegans* gene. *Genetics* **146:** 227–238.

Kennedy S, Wang D, Ruvkun G. 2004. A conserved siRNA-degrading RNase negatively regulates RNA interference in *C. elegans*. *Nature* **427:** 645–649.

Kumar S, Stecher G, Tamura K. 2016. MEGA7: Molecular Evolutionary Genetics Analysis version 7.0 for bigger datasets. *Mol Biol Evol* **33:** 1870–1874.

Lee RC, Hammell CM, Ambros V. 2006. Interacting endogenous and exogenous RNAi pathways in *Caenorhabditis elegans*. *RNA* **12:** 589–597.

Lee YS, Pressman S, Andress AP, Kim K, White JL, Cassidy JJ, Li X, Lubell K, Lim DH, Cho IS, et al. 2009. Silencing by small RNAs is linked to endosomal trafficking. *Nat Cell Biol* **11:** 1150–1156.

Manders EMM, Verbeek FJ, Ate JA. 1993. Measurement of co-localisation of objects in dual-colour confocal images. *J Microsc* **169:** 375–382.

Mello CC, Kramer JM, Stinchcomb D, Ambros V. 1991. Efficient gene transfer in *C. elegans*: extrachromosomal maintenance and integration of transforming sequences. *EMBO J* **10:** 3959–3970.

Patton JG, Franklin JL, Weaver AM, Vickers K, Zhang B, Coffey RJ, Ansel KM, Blelloch R, Goga A, Huang B, et al. 2015. Biogenesis, delivery, and function of extracellular RNA. *J Extracell Vesicles* **4:** 27494.

Pavelec DM, Lachowiec J, Duchaine TF, Smith HE, Kennedy S. 2009. Requirement for the ERI/DICER complex in endogenous RNA interference and sperm development in *Caenorhabditis elegans*. *Genetics* **183:** 1283–1295.

Petkovic M, Jemaiel A, Daste F, Specht CG, Izeddin I, Vorkel D, Verbavatz JM, Darzacq X, Triller A, Pfenninger KH, et al. 2014. The SNARE Sec22b has a non-fusogenic function in plasma membrane expansion. *Nat Cell Biol* **16:** 434–444.

Scott CC, Vacca F, Gruenberg J. 2014. Endosome maturation, transport and functions. *Semin Cell Dev Biol* **31:** 2–10.

Simmer F, Tijsterman M, Parrish S, Koushika SP, Nonet ML, Fire A, Ahringer J, Plasterk RHA. 2002. Loss of the putative RNA-directed RNA polymerase RRF-3 makes *C. elegans* hypersensitive to RNAi. *Curr Biol* **12:** 1317–1319.

Stagljar I, Korostensky C, Johnsson N, te Heesen S. 1998. A genetic system based on split-ubiquitin for the analysis of interactions between membrane proteins in vivo. *Proc Natl Acad Sci* **95:** 5187–5192.

Stalder L, Heusermann W, Sokol L, Trojer D, Wirz J, Hean J, Fritzsche A, Aeschimann F, Pfanzagl V, Basselet P, et al. 2013. The rough endoplasmatic reticulum is a central nucleation site of siRNA-mediated RNA silencing. *EMBO J* **32:** 1115–1127.

Tabara H, Grishok A, Mello CC. 1998. RNAi in *C. elegans*: soaking in the genome sequence. *Science* **282:** 430–431.

Tahbaz N, Kolb FA, Zhang H, Jaronczyk K, Filipowicz W, Hobman TC. 2004. Characterization of the interactions between mammalian PAZ PIWI domain proteins and Dicer. *EMBO Rep* **5:** 189–194.

Timmons L, Court DL, Fire A. 2001. Ingestion of bacterially expressed dsRNAs can produce specific and potent genetic interference in *Caenorhabditis elegans*. *Gene* **263:** 103–112.

Treusch S, Knuth S, Slaugenhaupt SA, Goldin E, Grant BD, Fares H. 2004. *Caenorhabditis elegans* functional orthologue of human protein h-mucolipin-1 is required for lysosome biogenesis. *Proc Natl Acad Sci* **101:** 4483–4488.

Ungar D, Hughson FM. 2003. SNARE protein structure and function. *Annu Rev Cell Dev Biol* **19:** 493–517.

Valadi H, Ekström K, Bossios A, Sjöstrand M, Lee JJ, Lötvall JO. 2007. Exosome-mediated transfer of mRNAs and microRNAs is a novel mechanism of genetic exchange between cells. *Nat Cell Biol* **9:** 654–659.

Voinnet O. 2013. MicroRNA and autophagy—*C. elegans* joins the crew. *EMBO Rep* **14:** 485–487.

Wählby C, Kamentsky L, Liu ZH, Riklin-Raviv T, Conery AL, O'Rourke EJ, Sokolnicki KL, Visvikis O, Ljosa V, Irazoqui JE, et al. 2012. An image analysis toolbox for high-throughput *C. elegans* assays. *Nat Methods* **9:** 714–716.

Winston WM, Molodowitch C, Hunter CP. 2002. Systemic RNAi in *C. elegans* requires the putative transmembrane protein SID-1. *Science* **295:** 2456–2459.

Winston WM, Sutherlin M, Wright AJ, Feinberg EH, Hunter CP. 2007. *Caenorhabditis elegans* SID-2 is required for environmental RNA interference. *Proc Natl Acad Sci* **104:** 10565–10570.

Zhang P, Zhang H. 2013. Autophagy modulates miRNA-mediated gene silencing and selectively degrades AIN-1/GW182 in *C. elegans*. *EMBO Rep* **14:** 568–576.

Zhao X, Yang H, Liu W, Duan X, Shang W, Xia D, Tong C. 2015. Sec22 regulates endoplasmic reticulum morphology but not autophagy and is required for eye development in *Drosophila*. *J Biol Chem* **290:** 7943–7951.